

JAFAR ESKANDARI JAM\*, Y. RAHMATI NEZHAD \*

## SEMI-ANALYTICAL SOLUTION OF FUNCTIONALLY GRADED CIRCULAR SHORT HOLLOW CYLINDER SUBJECT TO TRANSIENT THERMAL LOADING

In this paper, by using a semi-analytical solution based on multi-layered approach, the authors present the solutions of temperature, displacements, and transient thermal stresses in functionally graded circular hollow cylinders subjected to transient thermal boundary conditions. The cylinder has finite length and is subjected to axisymmetric thermal loads. It is assumed that the functionally graded circular hollow cylinder is composed of  $N$  fictitious layers and the properties of each layer are assumed to be homogeneous and isotropic. Time variations of the temperature, displacements, and stresses are obtained by employing series solving method for ordinary differential equation, Laplace transform techniques and a numerical Laplace inversion.

### Nomenclature

FGM	– functionally graded material
$N, i$	– total number of assumed layers and $i$ represents the $i$ -th layer $r^i < r < r^{i+1}$
$l, r_a, r_b$	– finite length, inner and outer radius
$t, r, z$	– time, radial and axial direction
$P, n$	– material property and non-negative volume fraction exponent
$m, c$	– the metal and ceramic
$V_m$	– the volume fraction of metallic constituent in the FGM

---

\* Composite Materials and Technology Center, MUT, Tehran, Iran

$E, \lambda, \alpha, \rho, C_v, \nu$	– Young's modulus, thermal conductivity coefficient, thermal expansion, density, specific heat capacity and Poisson's ratio
$E_0, \alpha_0, T_0$	– reference values of Young's modulus, thermal expansion coefficients and are temperature of the FGM cylinder
$T_a(z, t), T_b(z, t)$	– temperature distributions in the inner and outer surfaces of the hollow cylinder
$u^i, w^i$	– radial and axial displacements in the $i$ -th layer
$c_{kl}^i, \beta^i, T^{*i}, k^i$	– the elastic constants, thermoelastic coefficients, temperature and heat diffusivity in the $i$ -th layer
$\sigma_r^i, \sigma_\theta^i, \sigma_z^i, \tau_{r\theta}^i, \tau_{rz}^i, \tau_{z\theta}^i$	– radial, hoop, axial and shear stresses in the $i$ -th layer
$\varepsilon_r^i, \varepsilon_\theta^i, \varepsilon_z^i, \gamma_{rz}^i$	– radial, hoop, axial and shear strains in the $i$ -th layer
$L^{-1}, s$	– the inversion and variable of the Laplace transform

## 1. Introduction

One of the engineers concern in designing structures under multi-functional requirements, such as high temperature and large mechanical loads, is the uniformity of stress distribution and the time response of structures. For reducing the local stress concentrations induced by abrupt transitions in material properties, the transition between different materials is made gradually. To this end, functionally graded materials (FGMs) are recently used in structural components, such as finite length thick hollow cylinders, in order to optimize the thermal and mechanical loadings responses. Some of researchers have carried out analytical and computational studies of stresses, displacements and temperature in cylindrical shell made of FGM.

Using finite difference method, Awaji and Sivakuman [1] studied the transient thermal stresses of a FGM hollow circular cylinder, which is cooled by surrounding medium. A multi-layered material model was employed to solve the transient temperature field in a FGM strip with continuous and piecewise differentiable material properties by Jin [2]. Based on the multi-layered method, Kim and Noda [3, 4] researched unsteady thermoelastic problems of functionally graded infinite hollow cylinders by using a Green's function approach. Jabbari et al. [5] derived analytical solutions for one-dimensional steady-state thermoelastic problems of functionally graded circular hollow

cylinders in the case of material models expressed as power functions of  $r$ , and treated the two-dimensional thermoelastic problems of the functionally graded cylinder by using the Fourier transform. Tarn et al. [6] have studied the end effects of steady state heat conduction in a hollow or solid cylinder of FGM under two-dimensional thermal loads with arbitrary end conditions. Chen et al. [7] presented the sensitivity analysis of heat conduction for functionally graded materials and the steady state and transient problem treated with the direct method and the adjoint method.

Transient temperature field and associated thermal stresses in FGM have been determined by using a finite element-finite difference method by Wang et al. [8]. Shao and Wang [9] derived analytical solutions of mechanical stresses of a functionally graded circular hollow cylinder with finite length. Shao [10], by using a multi-layered approach based on the theory of laminated composites, presented the solutions of temperature, displacements, and thermal/mechanical stresses in a functionally graded circular hollow cylinder. The cylinder had finite length and was subjected to axisymmetric thermal and mechanical loads. The material properties were assumed to be temperature-independent and radially dependent, but were assumed to be homogeneous in each layer. A finite element-finite difference method was developed also to solve the time dependent temperature field in non-homogeneous materials such as FGMs by Wang et al. [11]. Jabbari et al. [12] presented the general theoretical analysis of three-dimensional mechanical and thermal stresses for a short hollow cylinder made of FGMs. The steady-state temperature, displacements, and stresses distributions were derived. The temperature and Navier equations are solved analytically, using the generalized Bessel function and Fourier series. Employing Laplace transform techniques and series solving method for ordinary differential equations, solutions for the time-dependent temperature and thermo-mechanical stresses are obtained in their study. Hosseini et al. [13] studied the transient heat conduction in functionally graded cylinder using an analytical method. Thermo-mechanical analysis of functionally graded hollow circular cylinders subjected to mechanical loads and linearly increasing boundary temperature is carried out by Shao and Ma [14]. Asgari and Akhlaghi [15] investigated the heat conduction equation in a 2D-FGM thick hollow cylinder with finite length by finite element method. Rahmati Nezhad et al. [16] presented semi-analytical solution of heat conduction equation using multilayered approach for an FGM thick short hollow cylinder.

The main objective of the present paper is to give transient thermal stress of FGM finite length thick hollow cylinders. Investigations into transient analysis of FGM thick hollow cylinders are more in plain strain condition. In addition, thermoelastic analyses of finite length FGM hollow cylinders are

under the steady thermal loads. To solve the transient heat conduction equation and Navier equations, it is assumed the cylinder is made of isotropic sub-cylinders, the continuity conditions for temperature, heat transfer, displacements and stresses between each layer are satisfied. We used series solution method for solving the ordinary differential equations and by employing Laplace transform techniques and numerical Laplace inverse method, solutions for the transient temperature and thermal stresses are obtained. The advantage of this method is its applicability to any material model suggested for functionally graded materials.

## 2. Problem formulation

In this section, volume fraction distribution in the radial is introduced. The governing equations of heat transfer and thermoelasticity in axisymmetric cylindrical coordinates are obtained.

### 2.1. Volume fraction and material distribution in FGM cylinder

We consider a thick functionally graded circular hollow cylinder as shown in Fig. 1. The cylinder is made of a combined ceramic-metal material. The inner surface of the cylinder is pure ceramic and the outer surface is pure metal. It is assumed that the FGM cylinder is composed of  $N$  fictitious layers and the properties of each layer are assumed to be homogeneous and isotropic. It should be noted that the material properties are assumed to be independent of temperature. As the temperature rise in this study is not too high, this assumption could be reasonable. Therefore, the effects of temperature on the material properties are not considered in the analysis. Material properties at each point can be obtained by using the linear rule of mixtures, in which a material property,  $P$ , in the FGM cylinder is determined by linear combination of volume fractions and material properties of the basic materials as

$$P = P_c + (P_m - P_c) V_m \quad (1)$$

where the subscripts  $m$  and  $c$  represent the metal and ceramic, respectively.  $V_m$  is the volume fraction of metallic constituent in the FGM, and is

$$V_m = \left( \frac{r - r_a}{r_b - r_a} \right)^n \quad (2)$$

Here  $n$  is a non-negative volume fraction exponent.

It should be noted that Poisson's ratio is assumed to be constant through the body. This assumption is reasonable because of the small differences between the Poisson's ratios of basic materials. The basic constituents of the

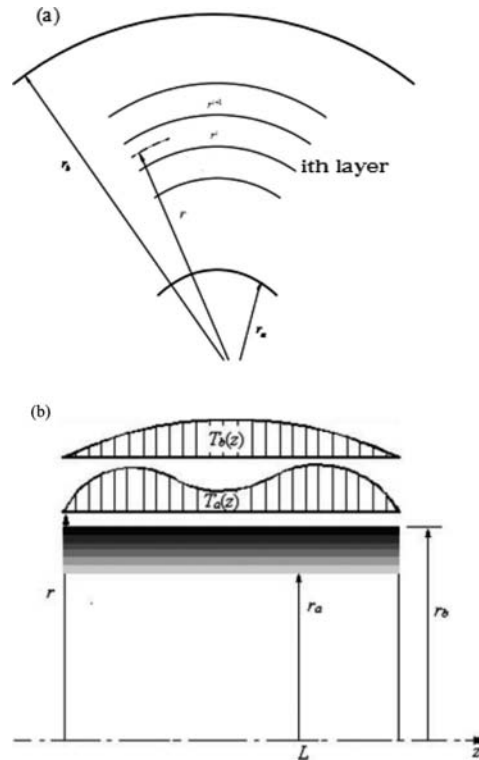


Fig. 1. The functionally graded circular hollow cylinder: (a) configuration of radial domain of hollow cylinder, (b) thermal loads

FGM cylinder are presented in Table 1. In this table  $E$ ,  $\lambda$ ,  $\alpha$ ,  $\rho$ ,  $C_v$  are Young's modulus, thermal conductivity coefficient, thermal expansion, density and specific heat capacity, respectively.

Table 1.

Thermoelastic properties of Alumina and Aluminum at 300 K [13]

Material	symbol	$E$ (GPa)	$\lambda$ (W/m·K)	$\alpha \left( \frac{1}{K} \right) \times 10^{-6}$	$C$ (J/kg·K)	$\rho \left( \frac{\text{kg}}{\text{m}^3} \right)$
Alumina (inner surface)	$c$	380	46	7.4	760	3800
Aluminum (outter surface)	$m$	70	250	23	896	2707

## 2.2. Governing equations

Consider a functionally graded circular hollow cylinder with finite length  $l$ , internal radius  $r_a$  and external radius  $r_b$  as shown in Fig. 1. The cylinder is simply supported on its two end edges. Temperatures on its two end surfaces

and initial temperature of cylinder are  $T_0$ . It is suddenly heated from the initial temperature  $T_0$  to axisymmetric transient temperature loads  $T_0 + T_a(z, t)$ ,  $T_0 + T_b(z, t)$  on the inner and outer surface. Because of axisymmetric geometry and loading, cylindrical coordinate's  $r$  and  $z$  are used in the analysis.

### 2.2.1. Geometric equations

The components of strain for each layer can be calculated from the following geometric relations:

$$\varepsilon_r^i = \frac{\partial u^i}{\partial r}, \quad \varepsilon_\theta^i = \frac{u^i}{r}, \quad \varepsilon_z^i = \frac{\partial w^i}{\partial z}, \quad \gamma_{rz}^i = \frac{\partial u^i}{\partial z} + \frac{\partial w^i}{\partial r}, \quad i = 1, 2, 3, \dots, N \quad (3)$$

where  $u^i$  and  $w^i$  are the radial and axial displacements in the  $i$ th layer  $r^i < r < r^{i+1}$ , respectively.  $N$  is the total number of assumed layers. The superscript  $i$  represents the  $i$ -th layer.

### 2.2.2. Constitutive equations

In the cylindrical coordinate system, thermoelastic constitutive relation of FGMs for each layer is as follows:

$$\sigma_r^i = c_{11}^i \frac{\partial u^i}{\partial r} + c_{12}^i \frac{u^i}{r} + c_{13}^i \frac{\partial w^i}{\partial z} - \beta^i T^{*i} \quad (4a)$$

$$\sigma_\theta^i = c_{12}^i \frac{\partial u^i}{\partial r} + c_{22}^i \frac{u^i}{r} + c_{23}^i \frac{\partial w^i}{\partial z} - \beta^i T^{*i} \quad (4b)$$

$$\sigma_z^i = c_{13}^i \frac{\partial u^i}{\partial r} + c_{23}^i \frac{u^i}{r} + c_{33}^i \frac{\partial w^i}{\partial z} - \beta^i T^{*i} \quad (4c)$$

$$\tau_{rz}^i = c_{55}^i \left( \frac{\partial u^i}{\partial z} + \frac{\partial w^i}{\partial r} \right) \quad i = 1, 2, 3, \dots, N \quad (4d)$$

where  $c_{kl}^i$ ,  $\beta^i$  and  $T^{*i}$  are the elastic constants, thermoelastic coefficients and temperature in the  $i$ -th layer, respectively and can be calculated from the following relations:

$$c_{11}^i = c_{22}^i = c_{33}^i = \frac{E^i(1-\nu)}{(1+\nu)(1-2\nu)} \quad (5a)$$

$$c_{12}^i = c_{13}^i = c_{23}^i = \frac{E^i\nu}{(1+\nu)(1-2\nu)} \quad (5b)$$

$$c_{55}^i = \frac{E^i}{2(1 + \nu)} \quad (5c)$$

$$\beta^i = \frac{E^i \alpha^i}{(1 - 2\nu)} \quad (5d)$$

$$T^{*i} = (T^i - T_0) \quad (5e)$$

where  $T_0, \nu$  are reference temperature and Poisson's ratio of the FGM cylinder. The shear stresses and strains in  $r\theta, \theta z$  planes are zero due to axisymmetric geometry and load distribution. Therefore  $\tau_{r\theta}^i = \tau_{z\theta}^i = 0$  and the other elastic constants,  $c_{44}^i, c_{66}^i$  in the stress matrix, are eliminated.

### 2.2.3. Heat conduction equations

The unsteady-state heat conduction equation of the FGM finite length hollow cylinder can be expressed as

$$\left( \frac{\partial^2}{\partial r^2} + \frac{1}{r} \frac{\partial}{\partial r} + \frac{\partial^2}{\partial z^2} - \frac{1}{k^i} \frac{\partial}{\partial t} \right) T^{*i} = 0 \quad (6)$$

$$k^i = \frac{\lambda^i}{\rho^i C_v^i}, \quad i = 1, 2, 3, \dots, N$$

$k^i$  is heat diffusivity of  $i$ -th layer of the FGM cylinder.

### 2.2.4. Equilibrium equations

Axial symmetry is assumed, so the formulation is reduced to two dimensions. By neglecting the body forces, the equilibrium equations in axisymmetric cylindrical coordinates could be obtained as:

$$\frac{\partial \sigma_r^i}{\partial r} + \frac{\partial \tau_{rz}^i}{\partial z} + \frac{\sigma_r^i - \sigma_\theta^i}{r} = 0 \quad (7a)$$

$$\frac{\partial \sigma_z^i}{\partial z} + \frac{\partial \tau_{rz}^i}{\partial r} + \frac{\tau_{rz}^i}{r} = 0, \quad i = 1, 2, 3, \dots, N \quad (7b)$$

where the superscripts 1 and  $N$  denote the inner and outer layers.

### 2.2.5. The initial and temperature boundary conditions

The initial and boundary conditions of temperature in the cylinder can be expressed as:

$$T^{*i}(r, z, 0) = 0, \quad i = 1, 2, 3, \dots, N \quad (8)$$

$$T^{*i}(r, 0, t) = T^{*i}(r, l, t) = 0, \quad i = 1, 2, 3, \dots, N \quad (9a)$$

$$T^{*1}(r_a, z, t) = T_a(z, t) \quad (9b)$$

$$T^{*N}(r_b, z, t) = T_b(z, t) \quad (9c)$$

where  $T_a(z, t)$  and  $T_b(z, t)$  are temperature distributions in the inner and outer surfaces of the hollow cylinder, respectively.

### 2.2.6. Temperature continuity conditions

The continuity conditions to be enforced at any interface between two layers are written as:

$$T^{*i-1}(r_i, z, t) = T^{*i}(r_i, z, t), \quad (10a)$$

$$\lambda^{i-1} \frac{\partial T^{*i-1}(r, z, t)}{\partial r} \Big|_{r=r_i} = \lambda^i \frac{\partial T^{*i}(r, z, t)}{\partial r} \Big|_{r=r_i}, \quad i = 2, 3, \dots, N \quad (10b)$$

### 2.2.7. Mechanical boundary conditions

The cylinder is simply supported on its two end edges, so the mechanical boundary conditions are assumed as:

$$u^i(r, 0, t) = 0, \quad \sigma_z^i(r, 0, t) = 0, \quad i = 1, 2, 3, \dots, N \quad (11a)$$

$$u^i(r, l, t) = 0, \quad \sigma_z^i(r, l, t) = 0, \quad i = 1, 2, 3, \dots, N \quad (11b)$$

$$\sigma_r^1(r_a, z, t) = q_a(z, t) = 0, \quad \tau_{rz}^1(r_a, z, t) = 0 \quad (11c)$$

$$\sigma_r^N(r_b, z, t) = q_b(z, t) = 0, \quad \tau_{rz}^N(r_b, z, t) = 0 \quad (11d)$$

### 2.2.8. Mechanical continuity conditions

The continuity conditions to be enforced at any interface between two layers are written as:

$$\sigma_r^{i-1}(r_i, z, t) = \sigma_r^i(r_i, z, t), \quad \tau_{rz}^{i-1}(r_i, z, t) = \tau_{rz}^i(r_i, z, t), \quad i = 2, 3, \dots, N \quad (12a)$$

$$u^{i-1}(r_i, z, t) = u^i(r_i, z, t), \quad w^{i-1}(r_i, z, t) = w^i(r_i, z, t), \quad i = 2, 3, \dots, N \quad (12b)$$

### 3. Series solution

The solution of Eq. (6) satisfying the boundary conditions (9) can be expressed as the form of Fourier series:

$$T^{*i}(r, z, t) = \sum_{n=1}^{\infty} F_n^i(r, t) \sin(\beta z), \quad \beta = \frac{n\pi}{l}, \quad i = 1, 2, 3, \dots, N \quad (13)$$

Substituting Eq. (13) into Eq. (6), one can obtain

$$\left[ \left( \frac{\partial^2}{\partial r^2} + \frac{1}{r} \frac{\partial}{\partial r} \right) - \beta^2 \right] F_n^i(r, t) = \frac{1}{k^i} \frac{\partial F_n^i(r, t)}{\partial t} \quad (14)$$

Considering the initial condition (8), Laplace transformation to Eq. (14) and boundary conditions (9) and continuity conditions (10) with respect to variable  $t$  is performed. It derives

$$\text{Laplace}\{F_n^i(r, t)\} = f_n^i(r, s) \quad (15)$$

$$\left[ \left( \frac{\partial^2}{\partial r^2} + \frac{1}{r} \frac{\partial}{\partial r} \right) - \beta^2 \right] f_n^i(r, s) = \frac{s}{k^i} f_n^i(r, s) \quad (16)$$

$$f_n^1(r_a, s) = G_a(s), \quad G_a(s) = L[T_{an}] = L \left[ \frac{2}{l} \int_0^l T_a(z, t) \sin(\beta z) dz \right] \quad (17a)$$

$$f_n^N(r_b, s) = G_b(s), \quad G_b(s) = L[T_{bn}] = L \left[ \frac{2}{l} \int_0^l T_b(z, t) \sin(\beta z) dz \right] \quad (17b)$$

$$f_n^{i-1}(r^i, s) = f_n^i(r^i, s) \quad (18a)$$

$$\lambda^{i-1} \frac{\partial f_n^{i-1}(r^i, s)}{\partial r} = \lambda^i \frac{\partial f_n^i(r^i, s)}{\partial r}, \quad i = 2, 3, \dots, N \quad (18b)$$

It can be seen that Eq. (16) is linear ordinary differential equation. According to the theory of linear ordinary differential equations, because all coefficients of Eq. (16) are analytical at point  $(r = r_b)$ , and can be expressed as Taylor series of  $(r - r_b)$ , so the solutions of Eq. (16) are also analytical at point  $(r = r_b)$ , and can be expressed as the following Taylor series

$$f_n^i(r, s) = \sum_{k=0}^{\infty} A_k^i(s) (r - r_b)^k \quad (19)$$

Substituting Eq. (19) into Eq. (16), and letting the coefficient of  $(r - r_b)^k$  equal zero, one can derive the following recurrence relations

$$\begin{aligned} A_2^i &= \frac{1}{2(r_b)} \left\{ \left( \beta^2 + \frac{s}{k^i} \right) (r_b) A_0^i - A_1^i \right\}, \quad k = 1, 2, \dots \\ A_{k+2}^i &= \frac{-1}{(k+1)(k+2)(r_b)} \left\{ (k+1)^2 A_{k+1}^i - \left( \beta^2 + \frac{s}{k^i} \right) (r_b) A_k^i + A_{k-1}^i \right\} \end{aligned} \quad (20)$$

Making use of Eq. (20), one can derive all coefficients  $A_k^i$  in series (19) by recursive computation. For  $k = 1$ , we first carry out the coefficient  $A_3^i$ , which is expressed by  $A_0^i$ ,  $A_1^i$  and  $A_2^i$ . Second, submitting the preceding derived coefficient into the expression of  $A_3^i$ , we can also obtain the relation expressed by  $A_0^i$ ,  $A_1^i$ . Continuing this recursive computation, similar expression of all coefficients  $A_k^i$  can be carried out. Considering a circular hollow cylinder composed of  $N$  fictitious layers, the total number of unknown constants ( $A_0^i$ ,  $A_1^i$ ), is  $2N$ . All unknown constants can be solved by Eqs. (17) and (18).

#### 4. Numerical Laplace inversion

To obtain the distribution of the temperature in the physical domain, it is necessary to perform Laplace inversion for the transformed temperature obtained when a sequence of values of  $s$  is specified. In this paper, an accurate and efficient numerical method is used to obtain the inversion of the Laplace transform. The inversion of the Laplace transform is defined as

$$L^{-1}[f_n^i(r, s)] = \frac{1}{2\pi i} \int_{a-i\infty}^{a+i\infty} e^{st} f_n^i(r, s) dt = F_n^i(r, t) \quad (21)$$

$a > 0$  is arbitrary, but is greater than the real parts of all the singularities of  $f_n^i(r, s)$ .

The numerical inversion of the Laplace transform [17] can be written

$$\begin{aligned} F_n^i(r, t) + Error(a, t, T) = & \frac{2 \exp(at)}{T} \left[ -\frac{1}{2} Re\{f_n^i(r, a)\} + \right. \\ & \left. \sum_{k=0}^{NSUM} \left( Re\{f_n^i(r, a + ik \frac{2\pi}{T})\} \cos(k \frac{2\pi}{T} t) - Im\{f_n^i(r, a + ik \frac{2\pi}{T})\} \sin(k \frac{2\pi}{T} t) \right) \right] \end{aligned} \quad (22)$$

In this numerical method, for good results, should

$$5 < aT < 10 \quad \& \quad 50 < NSUM < 5000$$

and in (22)

$$\begin{aligned} \text{if } |f(t)| < C &\Rightarrow |Error(a, t, T)| < \frac{C}{\exp(aT) - 1} \\ \text{for } aT = 8 &\Rightarrow |Error(a, t, T)| < 3.36 \times 10^{-4} \cdot C \end{aligned}$$

The advantages of this numerical method are twofold: first, the error bound on the inverse  $f(t)$  becomes independent of  $t$ , instead of being exponential in  $t$ ; second, and consequently, the trigonometric series obtained for  $F_n^i(r, t)$  in terms of  $f_n^i(r, s)$  is valid on the whole period  $2T$  of the series. Using of this numerical method, we have

$$F_n^i(r, t) = \sum_{k=0}^{\infty} A_k^i(t)(r - r_b)^k \quad (23)$$

The solutions of displacements that satisfying the mechanical boundary conditions (12a) and (12b) can be expressed as

$$u^i(r, z, t) = \sum_{n=1}^{\infty} \Phi_n^i(r, t) \sin(\beta z) \quad (24a)$$

$$w^i(r, z, t) = \sum_{n=0}^{\infty} \psi_n^i(r, t) \cos(\beta z) \quad , \quad \beta = \frac{n\pi}{L} \quad (24b)$$

Substituting Eqs. (4a)–(4c) into Eqs. (7a) and (7b), and using Eqs. (24a) and (24b) one can obtain Navier equations

$$\begin{aligned} &\left[ c_{11}^i \left( \frac{\partial^2}{\partial r^2} + \frac{1}{r} \frac{\partial}{\partial r} \right) - \frac{c_{22}^i}{r^2} + c_{55}^i \beta^2 \right] \Phi_n^i(r, t) \\ &- \left[ \beta (c_{13}^i + c_{55}^i) \frac{\partial}{\partial r} + (c_{13}^i - c_{23}^i) \frac{\beta}{r} \right] \psi_n^i(r, t) - \beta^i \frac{\partial F_n^i(r, t)}{\partial r} = 0 \end{aligned} \quad (25a)$$

$$\begin{aligned} &\left[ \beta (c_{13}^i + c_{55}^i) \frac{\partial}{\partial r} + (c_{55}^i + c_{23}^i) \frac{\beta}{r} \right] \Phi_n^i(r, t) \\ &+ \left[ c_{55}^i \left( \frac{\partial^2}{\partial r^2} + \frac{1}{r} \frac{\partial}{\partial r} \right) - c_{33}^i \beta^2 \right] \psi_n^i(r, t) - \beta \beta^i F_n^i(r, t) = 0 \end{aligned} \quad (25b)$$

Therefore, the boundary and mechanical continuity conditions be expressed as

$$c_{11}^1 \frac{\partial \Phi_n^1(r_a, t)}{\partial r} + c_{12}^1 \frac{\Phi_n^1(r_a, t)}{r_a} - c_{13}^1 \psi_n^1(r_a, t) - \beta^1 F_n^1(r_a, t) = 0 \quad (26a)$$

$$c_{11}^N \frac{\partial \Phi_n^N(r_b, t)}{\partial r} + c_{12}^N \frac{\Phi_n^N(r_b, t)}{r_b} - c_{13}^N \psi_n^N(r_b, t) - \beta^N F_n^N(r_b, t) = 0 \quad (26b)$$

$$\Phi_n^1(r_a, t) + \frac{\partial \psi_n^1(r_a, t)}{\partial r} = 0 \quad (27a)$$

$$\Phi_n^N(r_b, t) + \frac{\partial \psi_n^N(r_b, t)}{\partial r} = 0 \quad (27b)$$

$$\begin{aligned} & c_{11}^{i-1} \frac{\partial \Phi_n^{i-1}(r^i, t)}{\partial r} + c_{12}^{i-1} \frac{\Phi_n^{i-1}(r^i, t)}{r^i} - c_{13}^{i-1} \psi_n^{i-1}(r^i, t) - \beta^{i-1} F_n^{i-1}(r^i, t) \\ & = c_{11}^i \frac{\partial \Phi_n^i(r^i, t)}{\partial r} + c_{12}^i \frac{\Phi_n^i(r^i, t)}{r^i} - c_{13}^i \psi_n^i(r^i, t) - \beta^i F_n^i(r^i, t) \end{aligned} \quad (28a)$$

$$c_{55}^{i-1} \left\{ \Phi_n^{i-1}(r^i, t) + \frac{\partial \psi_n^{i-1}(r^i, t)}{\partial r} \right\} = c_{55}^i \left\{ \Phi_n^i(r^i, t) + \frac{\partial \psi_n^i(r^i, t)}{\partial r} \right\} \quad (28b)$$

$$\Phi_n^{i-1}(r^i, t) = \Phi_n^i(r^i, t), \quad i = 2, 3, \dots, N \quad (29a)$$

$$\psi_n^{i-1}(r^i, t) = \psi_n^i(r^i, t), \quad i = 2, 3, \dots, N \quad (29b)$$

$$\beta = \frac{n\pi}{L}$$

The solution of Eq. (25a) and (25b) can also be expressed as the following Taylor's series at the point of ( $r = r_b$ ):

$$\Phi_n^i(r, t) = \sum_{k=0}^{\infty} B_k^i(t)(r - r_b)^k \quad (30a)$$

$$\psi_n^i(r, t) = \sum_{k=0}^{\infty} D_k^i(t)(r - r_b)^k \quad (30b)$$

Substituting Eqs. (30) into Eqs. (25) and letting the coefficient of  $(r - r_b)^k$  equal zero, one can derive the following recurrence relations

$$\begin{aligned} & -2c_{11}^i(r_b)^2 B_2^i = (-c_{22}^i - \beta^2(r_b)^2 c_{55}^i) B_0^i + \beta(c_{13}^i - c_{23}^i)(r_b) D_0^i + c_{11}^i(r_b) B_1^i \\ & -\beta(c_{13}^i + c_{55}^i)(r_b)^2 D_1^i - \beta^i(r_b)^2 A_1^i \\ & -6c_{11}^i(r_b)^2 B_3^i = -2\beta^2 c_{55}^i(r_b) B_0^i - \beta(c_{13}^i - c_{23}^i) D_0^i + (c_{11}^i - c_{22}^i - \beta^2(r_b)^2 c_{55}^i) B_1^i \\ & +\beta[-3c_{13}^i - 2c_{55}^i + c_{23}^i](r_b) D_1^i - 2\beta^i(r_b) A_1^i + 6c_{11}^i(r_b) B_2^i \\ & -2\beta(c_{13}^i + c_{55}^i)(r_b)^2 D_2^i - 2\beta^i(r_b)^2 A_2^i \\ & -(k+1)(k+2)c_{11}^i(r_b)^2 B_{k+2}^i \\ & = (k+1)(2k+1)c_{11}^i(r_b) B_{k+1}^i + (k^2 c_{11}^i - c_{22}^i - \beta^2(r_b)^2 c_{55}^i) B_k^i \\ & -2\beta^2 c_{55}^i(r_b) B_{k-1}^i - \beta^2 c_{55}^i B_{k-2}^i \\ & -\beta(k+1)(c_{13}^i + c_{55}^i)(r_b)^2 D_{k+1}^i - \beta[2k(c_{13}^i + c_{55}^i) + c_{13}^i - c_{23}^i](r_b) D_k^i \\ & -\beta((k-1)(c_{13}^i + c_{55}^i) + c_{13}^i + c_{23}^i) D_{k-1}^i \\ & -(k+1)\beta^i(r_b)^2 A_{k+1}^i - 2k\beta^i(r_b) A_k^i - (k-1)\beta^i A_{k-1}^i, \quad k = 2, 3, \dots \end{aligned} \quad (31a)$$

$$\begin{aligned}
-2c_{55}^i(r_b)D_2^i &= \beta(c_{23}^i + c_{55}^i)B_0^i - \beta^2 c_{33}^i(r_b)D_0^i - \beta^i \beta(r_b)A_0^i \\
&+ \beta(r_b)(c_{13}^i + c_{55}^i)B_1^i + c_{55}^i D_1^i \\
-(k+1)(k+2)c_{55}^i(r_b)D_{k+2}^i &= \beta(k+1)(c_{13}^i + c_{55}^i)(r_b)B_{k+1}^i \\
&+ \beta \left[ k(c_{13}^i + c_{55}^i) + c_{55}^i + c_{23}^i \right] B_k^i \\
&+ (k+1)^2 c_{55}^i D_{k+1}^i - \beta^2 c_{33}^i(r_b)D_k^i - \beta^2 c_{33}^i D_{k-1}^i \\
&- \beta^i \beta(r_b)A_k^i - \beta^i \beta A_{k-1}^i, \quad k = 1, 2, \dots
\end{aligned} \tag{31b}$$

Using the recurrence relations (31a) and (31b), we have

$$B_k^i, D_k^i = G(B_0^i, B_1^i, D_0^i, D_1^i) \tag{32}$$

$B_0^i, B_1^i, D_0^i, D_1^i$  are unknown constants which can be determined by the boundary and continuity conditions, Eqs (26)–(29). Substituting Eqs. (30a) and (30b) into Eqs. (24a) and (24b), one can obtain the solutions for displacements. Then, substituting Eqs. (28a) and (28b) into Eqs. (4a)–(4d), the thermal stresses of the FGM circular hollow cylinder are obtained.

## 5. Implementation and validation

To verify the present solution, as the similar works to the present work are few, we use a finite length FGM cylinder under steady thermal loading. This problem has been solved analytically in Ref. [10] using series solution. Consider a thick hollow cylinder with simply supported end conditions in which the material distribution in radial direction varies from ceramic (Mullite) at the inner surface to metal (Molybdenum) at the outer surface with a power law function. The geometrical parameters and the temperature distribution along z-direction are:

$$\begin{aligned}
r_a &= 0.7, \quad r_b = 1, \quad L = 5, \quad n = 5, \quad N = 10 \text{ Layers} \\
T_a(z) &= 200 \sin\left(\frac{\pi z}{l}\right), \quad T_b(z) = 0
\end{aligned}$$

For solving the mentioned problem by semi-analytical method developed here as a transient problem, we suppose that the thermal boundary conditions act as initial condition and we suppose  $NSUM = 500$ ,  $aT = 8$ . Therefore, responses after a long time can be considered as the steady state results. Figure 2 shows results at all points for  $t = 10^5$  sec. Comparison of the results in Fig. 2 and Table 2 shows good agreement between two works at all points. The dimensionless value of temperature distribution at  $z = 2.5$  (m)

is shown in the Fig. 2. In addition, dimensionless values of temperature, radial displacement, radial stress, and tangential stress in a specified point are compared in Table 2.

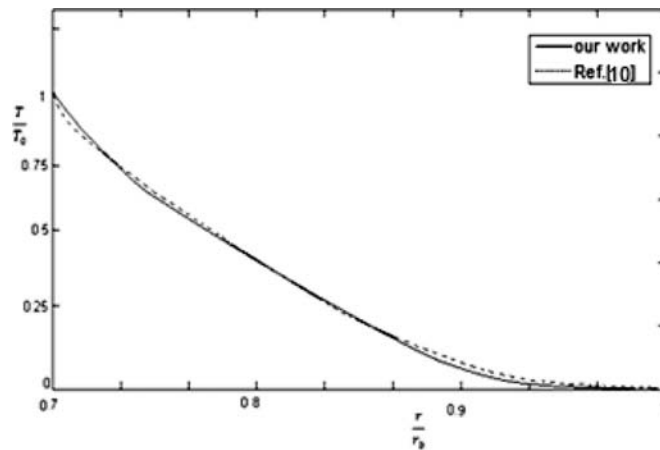


Fig. 2. Comparison of the temperature distribution at  $z = 2.5$  (m) present method and Ref. [10]

Table 2.

Comparison of the results between present method and Ref. [10]

$r/r_b = 0.85$ , $z/r_b = 2.5$	Present work	Ref.[10]
$T/T_0$	0.264	0.261
$u/T_0\alpha_0r_b$	0.422	0.428
$\sigma_r/E_0\alpha_0r_b$	-0.057	-0.053
$\sigma_\theta/E_0\alpha_0r_b$	0.428	0.431

It can be seen that  $NSUM = 500$ ,  $aT = 8$  gives accurate results. In this table,  $E_0$ ,  $\alpha_0$  are reference values of Young's modulus and thermal expansion coefficients of the FGM and can be briefly expressed as:

$$T_0 = 200 \text{ K}, \quad E_0 = 330 \text{ GPa}, \quad \alpha_0 = 4.9 \times 10^{-6} \frac{1}{\text{K}}$$

where  $T_0$  is reference temperature of FGM circular hollow cylinder.

## 6. Results and discussion

A thick hollow cylinder with  $r_a = 1$  m,  $r_b = 1.5$  m,  $L = 1$  m made of functionally graded material is investigated. Thermal loading and boundary

conditions are:

$$T^{*1}(r_a, z, t) = T_a(z, t) = 100(1 - \exp(at)) \sin\left(\frac{\pi z}{l}\right),$$

$$T^{*N}(r_b, z, t) = T_b(z, t) = 0,$$

$$\sigma_r^1(r_a, z, t) = q_a(z, t) = 0,$$

$$\sigma_r^N(r_b, z, t) = q_b(z, t) = 0,$$

$$T^{*i} = (T^i - T_0), \quad a = -2 \frac{1}{\text{sec}}, \quad T_0 = 300 \text{ K}, \quad N = 40 \text{ Layers}$$

In this part, the results for different values of power law exponent ( $n$ ) are presented and discussed. Those results are obtained for  $NSUM = 500$ ,  $aT = 8$  in Eq. (22). Figure 3 shows the temperature distribution through the cylinder at different times. Power law exponent of material distribution profile in radial direction is 5, i.e.  $n = 5$ .

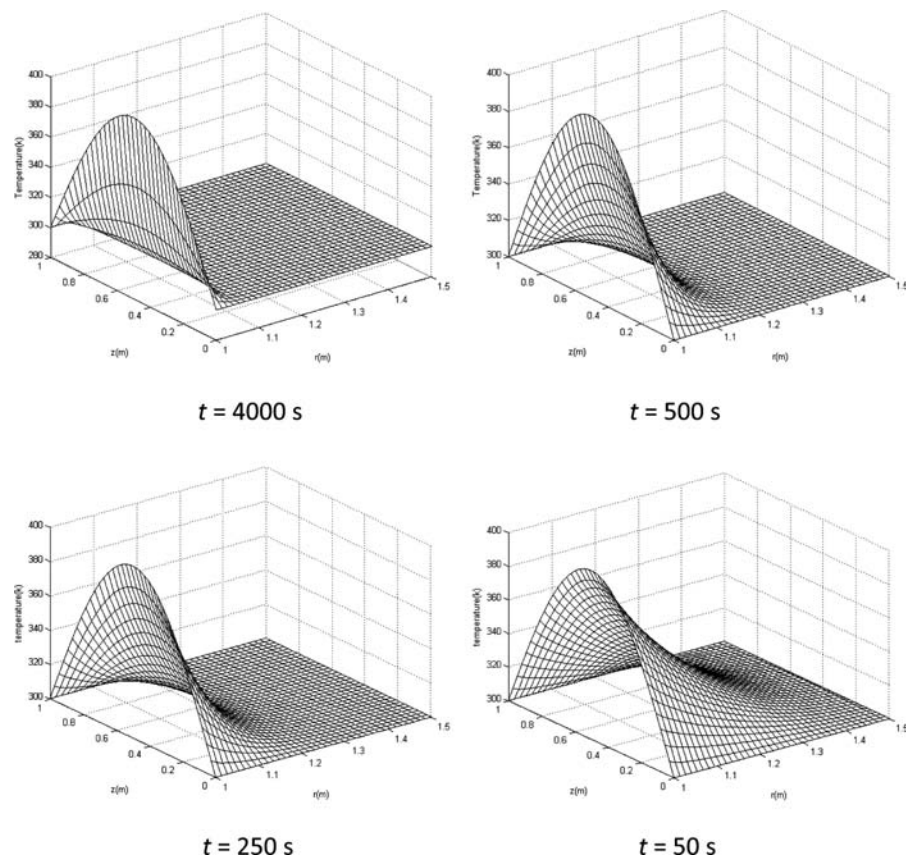


Fig. 3. Temperature distribution through the cylinder at different times for  $n = 5$

Due to the nonhomogeneity of the material properties, the variation of temperature is not linear through the thickness direction. The temperature near the inner surface reduces more quickly than that near the outer surface. In order to have a more clear and comprehensive observation, distributions of temperature through the cylinder at different times are illustrated in Fig. 4 for  $n = 2$

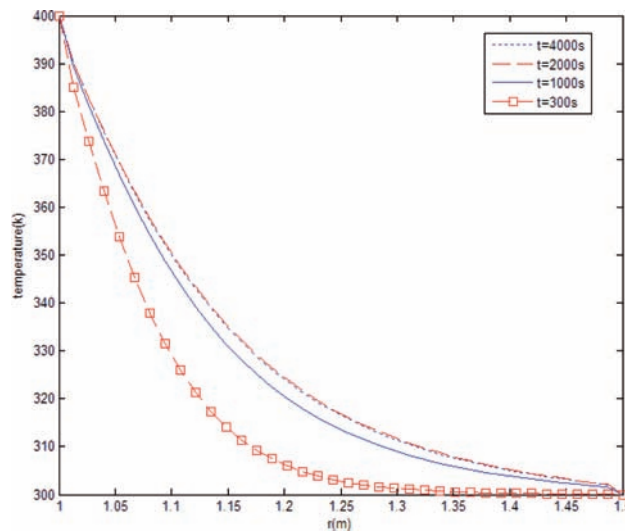


Fig. 4. Temperature distribution in the radial direction at  $z = 0.5$  m for different times,  $n = 2$

Radial distribution of temperature in the middle of the cylinder's length at a specified time ( $t = 4000$  s) is shown in the Fig. 6 for different material distributions.

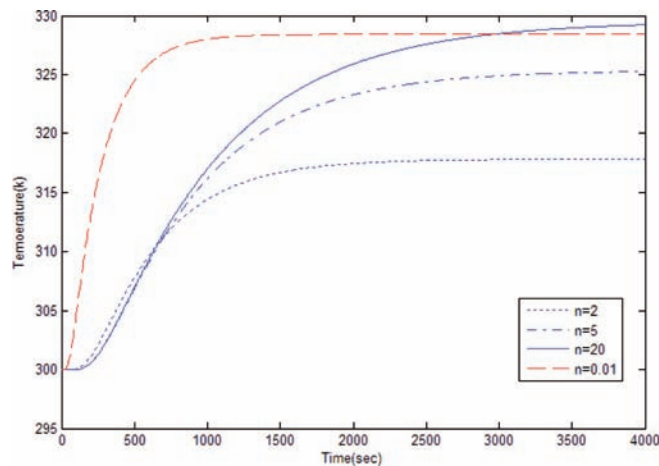


Fig. 5. Transient temperature at  $z = 0.5$  m,  $r = 1.25$  m for different material distributions

It is clear that the time responses are affected by material distribution tailoring. The same results are plotted for  $z = 0.5$  m in Fig. 5. It can be seen that, when increasing the power law exponent, the steady temperature of the specified point increases and also the temperature will become steady later.

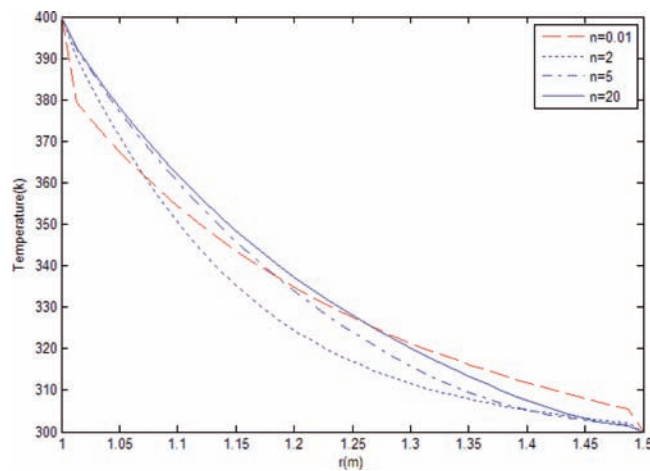


Fig. 6. Temperature distribution through the FGM cylinder for different power law exponents in the radial direction at  $z = 0.5$  m after 4000 s

It is evident from the figures that both of the amplitude and time delay of the responses are strongly affected by the material distribution power ( $n$ ). It can be seen that in the same conditions the temperature distribution is different. The lower the value of  $n$ , the lower the temperature is near the outer surface. Distributions of components of displacement caused by thermal loading after 4000 s are shown in the Figs. 7 and 8.

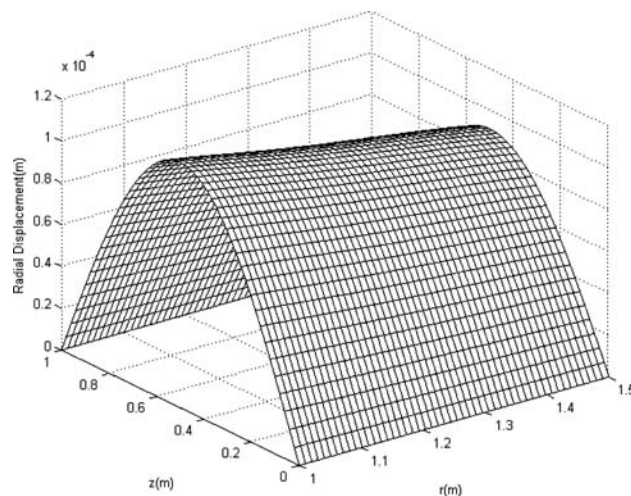


Fig. 7. Radial displacement distribution through the cylinder after 4000 s,  $n = 5$

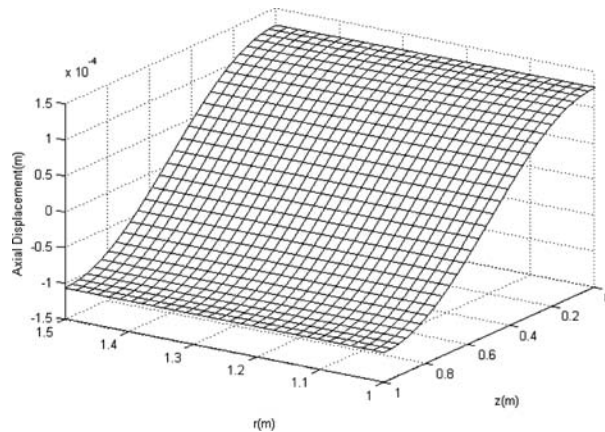


Fig. 8. Axial displacement distribution through the cylinder after 4000 s,  $n = 2$

According to the assumed boundary conditions, the radial displacement at two ends of the cylinder is zero and radial displacement is symmetric about the section  $z = 0.5$  m and the axial displacement is antisymmetric about the section, due to the assumed thermal loads. It can be seen from Fig. 9 that the radial stress at the outer and inner surface is reached to zero and

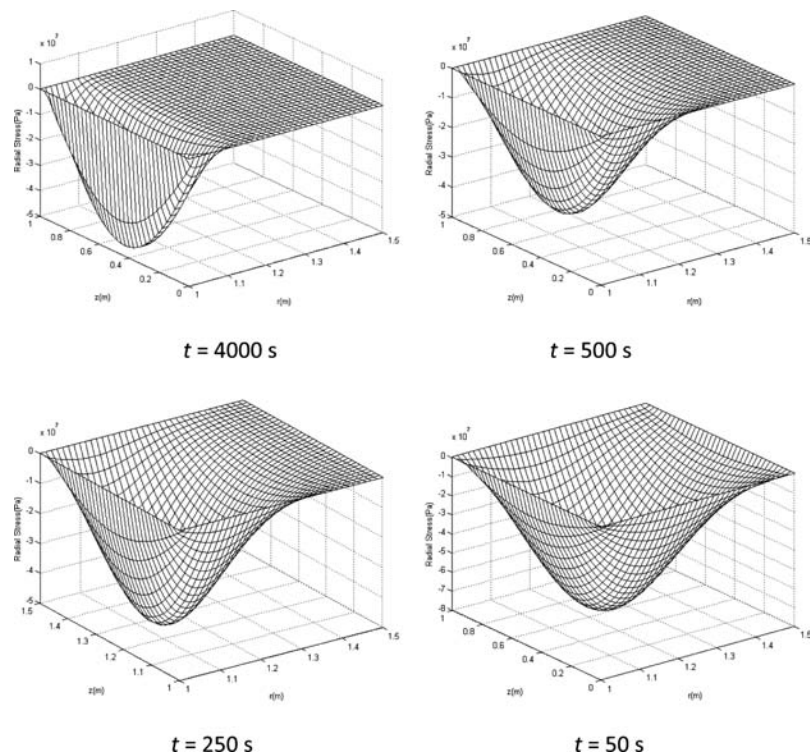


Fig. 9. Radial stress distribution through the cylinder at different times,  $n = 5$

radial stress is symmetric about the section  $z = 0.5$  m. This happens because of the assumed boundary conditions. According to this figure, the radial stress has negative value due to nature of loading.

It can be seen that increasing the power law exponent, the steady radial stress of the specified point increases and also the radial stress will become steady later.

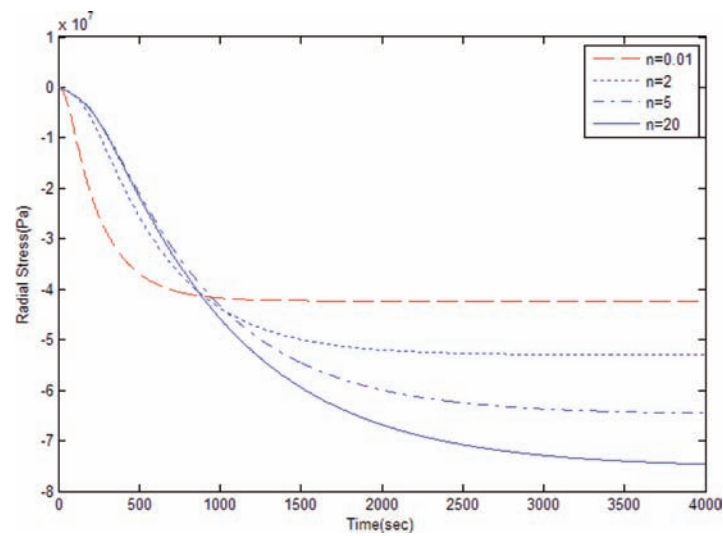


Fig. 10. Transient Radial Stress at  $z = 0.5$  m,  $r = 1.25$  m for different material distributions

The distributions of hoop stress and axial stress through the cylinder are presented in Figs. 11, 12, 13 and 14 for different times.

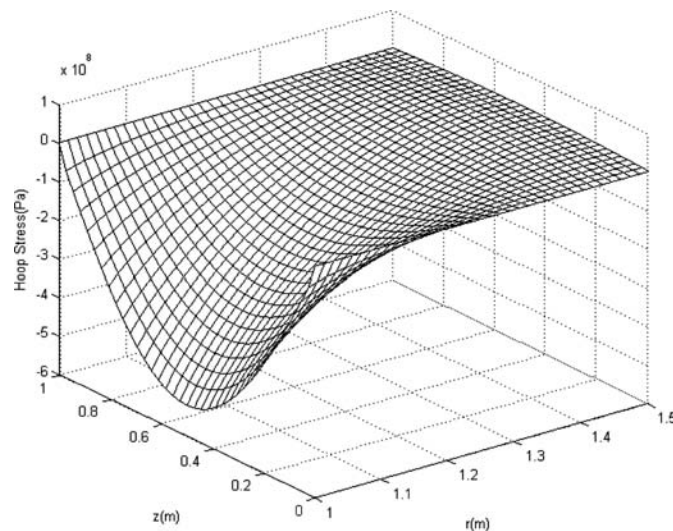


Fig. 11. Hoop Stress distribution through the cylinder after 4000 s, for  $n = 5$

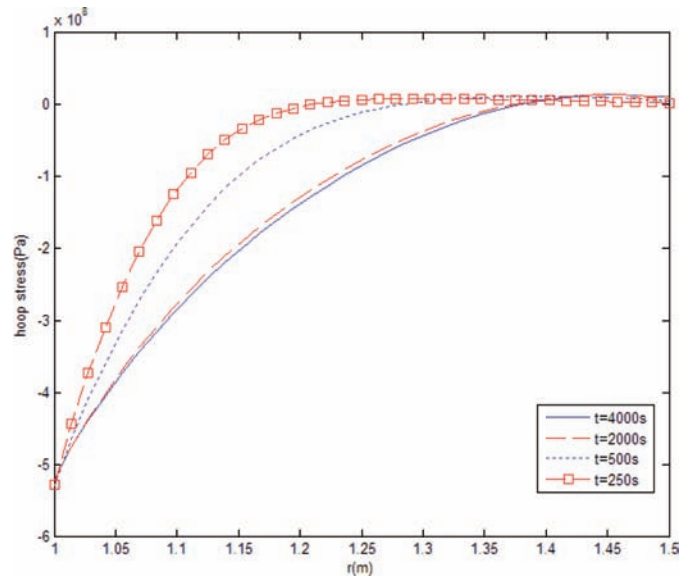


Fig. 12. Hoop Stress distribution in the radial direction and in  $z = 0.5$  m for different times,  $n = 5$

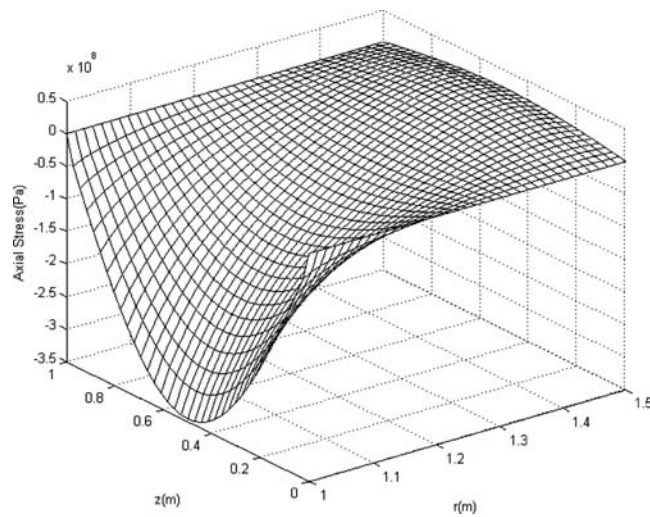


Fig. 13. Axial Stress distribution through the cylinder after 4000 s for  $n = 5$

It is seen that absolute values of the axial and circumferential thermal stresses increase with time and approaches to the maximum values at steady state.

Figure 15 shows the shear stress distribution through the cylinder at different times. Power law exponent of material distribution profile in radial direction is 5, i.e  $n = 5$ .

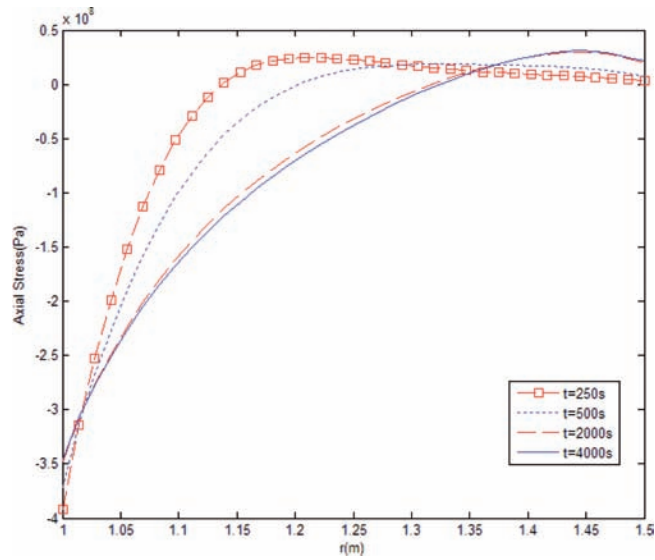


Fig. 14. Axial Stress distribution in the radial direction and in  $z = 0.5$  m for different times,  $n = 5$

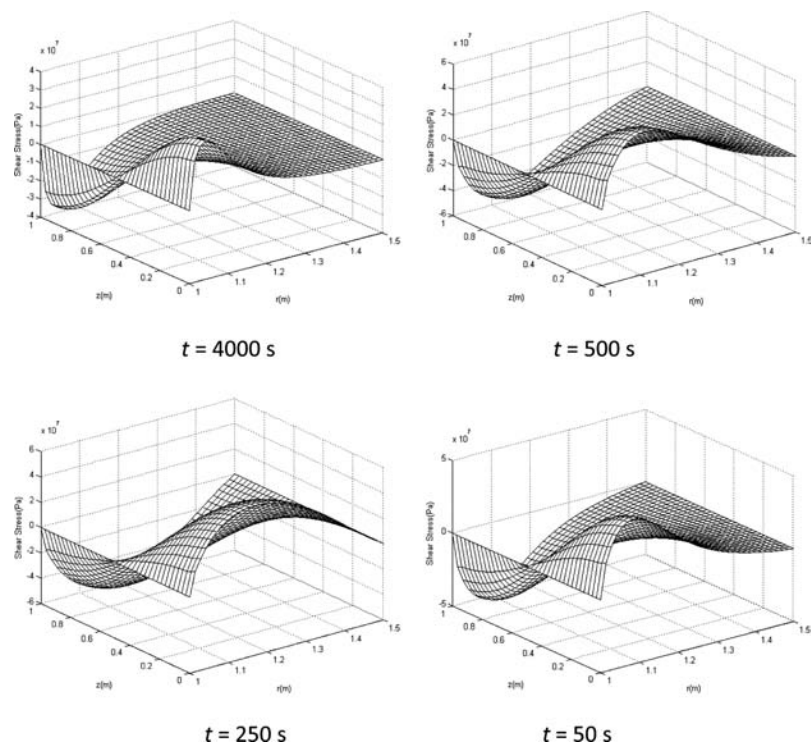


Fig. 15. Shear Stress distribution through the cylinder at different times for  $n = 5$

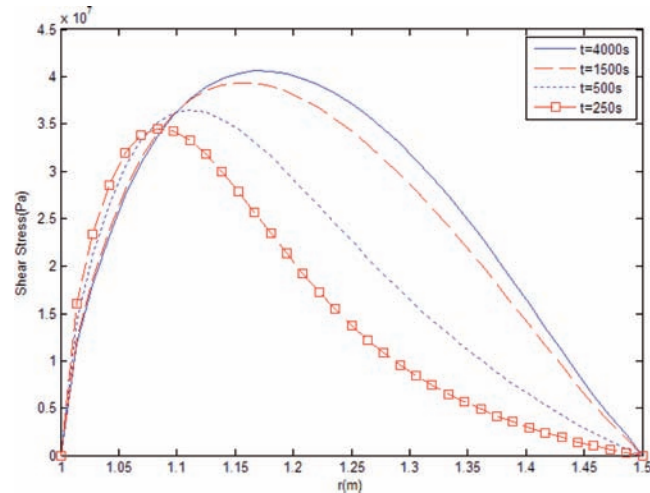


Fig. 16. Shear Stress distribution in the radial direction and in  $z = 0.25$  m for different times,  $n = 5$

Variations of shear stress with time in lower edges of the cylinder are illustrated in Fig. 17. As it is mentioned before, stress distributions are strongly influenced by the material composition profile. In other words, the time response, the maximum amplitude and the uniformity of stress distributions through the cylinder can be modified to a required manner by selecting appropriate material distribution profile.

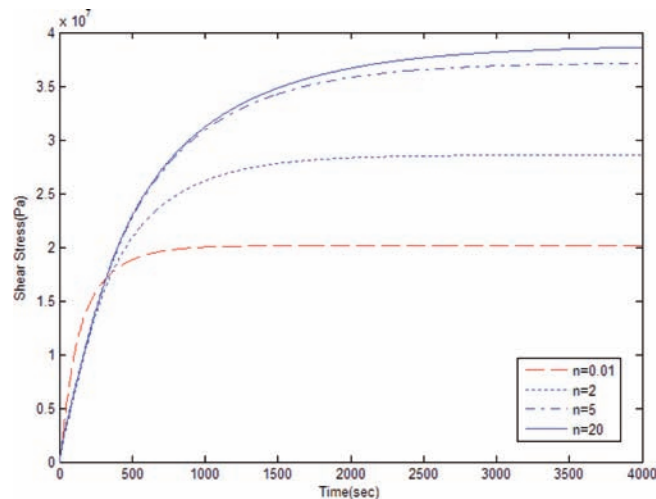


Fig. 17. Transient Shear Stress at  $z = 0.25$  m,  $r = 1.25$  m for different material distributions

As it is seen in the results, the maximum magnitude of axial stress is larger than that of radial stress, and smaller than that of hoop stress. The

maximum magnitude of shear stress is much smaller than that of normal stresses.

## 7. Concluding remarks

By semi-analytical method based on the theory of laminated composites, we analyzed transient thermal stress in a functionally graded short circular hollow cylinder. Using Laplace transform technique and numerical Laplace inverse method and series solving method for ordinary differential equation, solutions of time-dependent temperature, displacements, and unsteady thermal stresses of FGM hollow cylinders and variations of different parameters with volume fraction exponent are obtained. As an illustration, we carried out numerical calculations for the functionally graded circular hollow cylinder made of Alumina and Aluminum. The series solutions (14) and (28) suggested in this paper are only suitable for the boundary conditions that the temperature is zero at the two ends. For other temperature boundary conditions, one can also find suitable forms of series solutions to satisfy both the temperature and simply supported boundary conditions. The advantage of this method is its applicability to any material model suggested for functionally graded materials.

Manuscript received by Editorial Board, May 06, 2012;  
final version, April 20, 2014.

## REFERENCES

- [1] Awaji H., Sivakuman R.: Temperature and stress distributions in a hollow cylinder of functionally graded material: the case of temperature- dependent material properties. *J. Am. Ceram. Soc* 2001, 84, 059-1065.
- [2] Jin Z. H.: An asymptotic solution of temperature field in a strip of a functionally graded material, *Int Common strip of a functionally graded material. Int. Common Heat Mass Trans* 2002, 29(7), 887-895.
- [3] Kim K.S., Noda N.: Green's function approach to unsteady thermal stresses in an infinite hollow cylinder of functionally graded material. *Acta Mech* 2002, 156, 145-61.
- [4] Kim K.S., Noda N.: A Green's function approach to the deflection of a FGM plate under transient thermal loading. *Arch Appl Mech* 2002, 72, 127-37.
- [5] Jabbari M., Sohrabpour S., Eslami M. R.: Mechanical and thermal stresses in functionally graded hollow cylinder due to radially symmetric loads. *Int J Pressure Vessels Piping* 2002, 79, 493-7.
- [6] Tarn J.Q., Wang Y.M.: End effects of heat conduction in circular cylinders of functionally graded materials and laminated composites. *Int J Heat Mass Transf* 2004, 47, 5741-5747.
- [7] Chen B., Tong L.: Sensivity analysis of heat conduction for functionally graded materials. *Mater Des* 2004, 25, 663-672.
- [8] Wang B.L., Mai Y.W., Zhang X.H.: Thermal shock resistance of functionally graded materials. *Acta Mater* 2004, 52, 4961-4972.

- [9] Shao Z.S., Fan L.F., Wang T.J.: Analytical solutions of stresses in functionally graded circular hollow cylinder with finite length. *Key Eng Mater* 2004, 261-263, 651-6.
- [10] Shao Z.S.: Mechanical and thermal stresses of a functionally graded circular hollow cylinder with finite length. *Int. J. Press. Vessels Piping* 2005, 82, 155-163.
- [11] Wang B.L., Tian Z.H.: Application of finite element-finite difference method to the determination of transient temperature field in functionally graded materials. *Finite Elem. Anal. Des* 2005, 41, 335-349.
- [12] Jabbari M., Mohazzab A.H., Bahtui A., Eslami M.R.: Analytical solution for three dimensional stresses in a short length FGM hollow cylinder. *ZAMM. Z. Angew. Math. Mech* 2007, 87, 413-429.
- [13] Hosseini M., Akhlaghi M., Shakeri M.: Transient heat conduction in functionally graded thick hollow cylinders by analytical method. *Heat Mass Transf* 2007, 43, 669-675.
- [14] Shao Z.S., Ma G.W.: Thermo-mechanical stresses in functionally graded circular hollow cylinder with linearly increasing boundary temperature. *Compos Struct* 2008, 83(3), 259-265.
- [15] Asgari M., Akhlaghi M.: Transient heat conduction in two-dimensional functionally graded hollow cylinder with finite length. *Heat Mass Transfer* 2009, 45, 1383-1392.
- [16] Rahmati Nezhad Y., Asemi K., Akhlaghi M.: Transient solution of temperature field in functionally graded hollow cylinder with finite length using multi layered approach. *Int J Mech Mater Des* 2011, 7, 71-82.
- [17] Durbin F.: Numerical inversion of Laplace transforms an efficient improvement to Dubner and Abate's method. *The Computer Journal*, 1973, 371-376.

**Półanalityczne rozwiązanie dla krótkiego, wydrążonego, kolistego cylindra gradientowego  
poddanego przejściowemu obciążeniu termicznemu**

S t r e s z c z e n i e

W artykule zaprezentowano rozwiązanie dla temperatury, przemieszczeń i naprężeń w stanie nieustalonym w krótkich, wydrążonych, kolistych cylindrach gradientowych przy warunkach brzegowych odpowiadających przejściowemu obciążeniu termicznemu. Rozwiązanie uzyskano metodą półanalityczną opartą na podejściu wielowarstwowym. Rozważany cylinder ma skończoną długość i jest poddany obciążeniom termicznym o symetrii osiowej. Zakłada się, że wydrążony, kolisty cylinder gradientowy składa się z  $N$  fikcyjnych warstw, a właściwości każdej z warstw są izotropowe i jednorodne. Zmiany w czasie temperatury, przemieszczeń i naprężeń uzyskano wykorzystując metodę rozwinięcia na szereg dla zwyczajnych równań różniczkowych, metody transformacji Laplace'a i metodę cyfrową odwrotnego przekształcania Laplace'a.